

GTR-Mamba: Geometry-to-Tangent Routing Mamba for Hyperbolic POI Recommendation

Zhuoxuan Li*

College of Computer Science and
Technology, Tongji University
Shanghai, China
li_zhuoxuan@outlook.com

Jieyuan Pei*

College of Information Engineering,
Zhejiang University of Technology
Hangzhou, China
peijieyuan@zjut.edu.cn

Tangwei Ye

College of Computer Science and
Technology, Tongji University
Shanghai, China
yetw@tongji.edu.cn

Zhongyuan Lai

Shanghai Ballsnow Intelligent
Technology Co., Ltd
Shanghai, China
zhongyuan.lai@ballsnow.com

Zihan Liu

College of Computer Science and
Technology, Tongji University
Shanghai, China
tongjilzh@gmail.com

Fengyuan Xu

Hunan University
Changsha, China
xufengyuan126@gmail.com

Qi Zhang

College of Computer Science and
Technology, Tongji University
Shanghai, China
zhangqi_cs@tongji.edu.cn

Liang Hu[†]

College of Computer Science and
Technology, Tongji University
Shanghai, China
rainmilk@gmail.com

Abstract

Next Point-of-Interest (POI) recommendation is a critical task in modern Location-Based Social Networks (LBSNs), aiming to model the complex decision-making process of human mobility to provide personalized recommendations for a user’s next check-in location. Existing hyperbolic POI recommendation models, predominantly based on rotations and graph representations, have been extensively investigated. Although hyperbolic geometry has proven superior in representing hierarchical data with low distortion, current hyperbolic sequence models typically rely on performing recurrence via expensive Möbius operations directly on the manifold. This incurs prohibitive computational costs and numerical instability, rendering them ill-suited for trajectory modeling. To resolve this conflict between geometric representational power and sequential efficiency, we propose GTR-Mamba, a novel framework featuring Geometry-to-Tangent Routing. GTR-Mamba strategically routes complex state transitions to the computationally efficient Euclidean tangent space. Crucially, instead of a static approximation, we introduce a Parallel Transport (PT) mechanism that dynamically aligns tangent spaces along the trajectory. This ensures geometric consistency across recursive updates, effectively bridging the gap between the curved manifold and linear tangent operations. This process is orchestrated by an exogenous spatio-temporal channel, which explicitly modulates the SSM discretization parameters. Extensive experiments on three real-world datasets demonstrate that GTR-Mamba consistently outperforms state-of-the-art baselines in next POI recommendation.

CCS Concepts

• Information systems → Recommender systems.

*Both authors contributed equally to this research.

[†]Corresponding author

Keywords

POI Recommendation, Hyperbolic Mamba, Hyperbolic Space

1 Introduction

Point-of-Interest (POI) refers to a location that a user may find attractive or valuable. The proliferation of web-based location services and online social platforms [33, 42, 50] has generated vast amounts of user-generated, geotagged content. This rich spatio-temporal data, such as check-ins and shared locations, makes it possible to predict places a user is likely to visit based on their preferences and contextual signals, fueling research on personalized next POI recommendation within the field of spatio-temporal data mining. This task is inherently challenging due to the complex interplay between users’ hierarchical preferences and their dynamic, context-driven behaviors.

Existing recommendation systems are often based on sequential methods that personalize the processing of contextual information to better capture user preferences [1, 2, 40]. Furthermore, given the powerful capability of Graph Neural Networks (GNNs) [20, 31, 47] in integrating geographical information, they have been widely used in the task of next POI recommendation. Concurrently, recent breakthroughs in structured state-space sequence (S4) models have brought about significant efficiency improvements in sequential modeling. In particular, the Mamba architecture has gained significant prominence for its linear scaling capabilities [6, 17, 32]. However, these studies uniformly model user trajectories in Euclidean space, which struggle to effectively capture the inherent hierarchical and tree-like structures embedded in check-in behaviors.

In contrast, hyperbolic space naturally aligns with these latent hierarchies. Characterized by its negative curvature and exponential volume growth, it serves as an ideal inductive bias for modeling

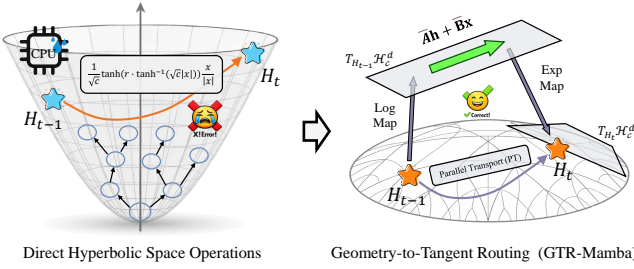


Figure 1: (Left) Direct hyperbolic recurrence. (Right) Proposed GTR-Mamba with geometry-to-tangent routing.

power-law distributions [29, 53]. In POI scenarios, hyperbolic embeddings can effectively organize multi-granular semantics (e.g., regions, categories, and POIs) and capture long-tail relationships within a low-dimensional space. Existing literature has explored embeddings in hyperbolic space [11, 25, 30], establishing it as a natural choice for modeling hierarchical data. These studies, often integrating hyperbolic geometry with rotation-based methods or variational graph auto-encoders, have demonstrated promising results. However, a critical gap remains in Sequential Modeling within current hyperbolic recommendation frameworks. Most existing works focus predominantly on static graph representations. The few attempts to construct hyperbolic sequence models typically rely on performing heavy Möbius operations directly on the manifold. This prohibitive computational cost and potential numerical instability severely constrain their scalability in scenarios involving long trajectories and large-scale candidate sets.

To address this fundamental conflict between the representational benefits of hyperbolic geometry and the efficiency of sequence modeling, we propose GTR-Mamba, a novel framework featuring Geometry-to-Tangent Routing. As illustrated in Figure 1, we design a novel Mamba layer that executes state updates within the computationally efficient Euclidean tangent space. Crucially, to mitigate the precision loss caused by tangent space approximation, we introduce a Parallel Transport (PT) mechanism. As the reference point changes dynamically, this mechanism rigorously transports the hidden vector from the previous tangent space to the current one, thereby maintaining geometric consistency across recursive steps. Furthermore, the discretization and update of the internal State Space Model (SSM) are explicitly driven by exogenous spatio-temporal conditions to adapt to irregular time intervals and contextual shifts. Overall, GTR-Mamba retains the superiority of hyperbolic representation while balancing efficiency and training stability in long-trajectory scenarios.

Our contributions are summarized as follows:

- We propose a novel hyperbolic Mamba layer that routes complex dynamic sequence updates to the computationally stable and efficient Euclidean tangent space for execution, while ensuring geometric fidelity via a Parallel Transport mechanism.
- We propose a context-explicit driven variable-step selective SSM, where internal dynamic state transitions adaptively adjust based on external spatiotemporal signals to address complex temporal and contextual shifts.

- Extensive experiments were conducted on three real-world LBSN datasets. The results confirm that our proposed GTR-Mamba model demonstrates superior overall performance compared to state-of-the-art baseline methods.

2 Related Work

2.1 Next POI Recommendation

Next Point-of-Interest (POI) recommendation often relies on modeling the complex transitional and sequential patterns within users’ historical check-ins. Leveraging the powerful deep modeling capabilities of deep neural networks, sequential models such as LSTM or RNN have been employed to treat the POI task as a sequence prediction problem [10, 24, 38, 45]. Concurrently, variants of the attention mechanism [9, 27, 48, 59] have been widely adopted due to their ability to focus on more critical parts of historical spatio-temporal information, thereby integrating richer contextual representations. Graph Neural Networks (GNNs) [20, 31, 43, 44, 47, 49] have also achieved significant success by further modeling geographical dependencies through neighborhood aggregation. Notably, some research has already recognized the importance of hierarchical structures for the POI recommendation task, including the introduction of auxiliary information such as POI categories [56, 58, 60] and geographical regions [21, 22, 46] to enhance recommendation performance. Furthermore, tree-based methods [2, 5, 16, 26] have also been proposed, as trees inherently possess a hierarchical structure.

Owing to Mamba’s formidable long-sequence modeling capabilities, several Mamba-based methods have recently been introduced. For instance, Chen et al. [6] leverage a combination of hierarchical geographical encoding and Mamba to achieve awareness of geographical sequences, while Qin et al. [32] utilize Mamba and the GaPPO operator to extend the state space for modeling multi-granularity spatio-temporal transitions. Although these recommendation methods have achieved excellent results, these state-of-the-art models predominantly operate in Euclidean space, which inherently struggles to preserve the underlying hierarchical and tree-like structures of human mobility.

2.2 Hyperbolic Representation Learning

Hyperbolic geometry has been extensively adopted in recommendation systems due to its superior capacity for modeling hierarchical structures [35]. Its applications span diverse domains, including knowledge-aware [7, 8], social [39, 55], session-based [14], and news recommendation [41]. Notably, hyperbolic collaborative filtering [19, 51] has demonstrated significant improvements over Euclidean baselines. In POI recommendation, HME [11] embeds interactions into a Poincaré ball, while recent works like HMST [30] and HVGAE [25] further advance this by utilizing hyperbolic rotations and variational graph autoencoders to capture multi-semantic transitions. However, these methods largely focus on static node representation or graph structures, often neglecting the efficient modeling of long-term sequential evolution.

To address temporal dynamics, recent research has integrated hyperbolic geometry into sequence encoders. Early attempts like HVACF [34] and the work by Patil et al. [28] introduced hyperbolic manifolds into user-item representation learning and pooled feature projection. To handle longer sequences, Hypformer [52] adapts

Transformer attention to Lorentz space, though it retains high computational complexity. More recently, geometry-aware methods like HMamba [61] and Hybrid-Emba3D [23] have explored linear-complexity architectures. Nevertheless, existing hyperbolic SSMS typically rely on computationally intensive Möbius operations for state updates, leading to higher per-step overhead in practice.

3 Preliminary

3.1 Basic Definition

Let \mathcal{U} , \mathcal{P} , \mathcal{C} , and \mathcal{R} be the sets of users, POIs, categories, and regions, respectively, where $|\mathcal{P}|$ is the total number of POIs. Each POI is associated with location information, represented by geographical coordinates, and category information that reflects its function. The regions are constructed by partitioning the entire geographical area based on the collected coordinates, which determines the region to which each POI belongs.

A check-in, denoted as $s = (u, p, t, c, r)$, records the event of a user $u \in \mathcal{U}$ visiting a specific POI $p \in \mathcal{P}$ at a timestamp t . Here, $c \in \mathcal{C}$ and $r \in \mathcal{R}$ represent the category and region of POI p , respectively. We represent the check-in sequence of a user u as $\mathcal{S}_u = \{s_1, s_2, \dots, s_{l_u}\}$, where s_i is the i -th check-in of user u , and l_u is the length of the sequence \mathcal{S}_u .

Given a user's historical check-in sequence \mathcal{S}_u , the objective of next POI recommendation is to predict the POI p_{l_u+1} that the user u is most likely to visit next.

3.2 Hyperbolic Space

Let \mathbb{H}_c^d denote a d -dimensional hyperbolic space with negative curvature $-1/c < 0$, where $c > 0$. In this paper, we adopt the Lorentz model embedded in \mathbb{R}^{d+1} . The d -dimensional Lorentz model is defined as a Riemannian manifold with constant negative curvature $-1/c$: $\mathbb{L}_c^d = (\mathbb{H}_c^d, g_c^d)$, where $\mathbb{H}_c^d = \{x \in \mathbb{R}^{d+1} : \langle x, x \rangle_L = -c; x_0 > 0\}$, $g_c^d(u, v) = \langle u, v \rangle_L$. We adopt the convention where the time coordinate is first: $x = (x_0, x_1, \dots, x_d)$, with x_0 being the temporal component. The Lorentzian inner product $\langle \cdot, \cdot \rangle_L$ is given by $\langle x, y \rangle_L = -x_0 y_0 + \sum_{i=1}^d x_i y_i$. The commonly used squared Lorentz distance [18] is defined as:

$$d_L^2(x, y) := -2c - 2\langle x, y \rangle_L. \quad (1)$$

This distance metric captures the hyperbolic geometry and is effective for representing hierarchical relationships.

Tangent space and base-point maps. For any point $x \in \mathcal{H}_c^d$, there exists a d -dimensional vector space $T_x \mathbb{H}_c^d$, known as the tangent space at x [29]. The exponential map $\exp_x(\cdot) : T_x \mathbb{H}_c^d \rightarrow \mathcal{H}_c^d$ and logarithmic map $\log_x(\cdot) : \mathcal{H}_c^d \rightarrow T_x \mathbb{H}_c^d$ transform between the tangent space and the manifold [12]. Importantly, the subscript in $\exp_x(\cdot)$ and $\log_x(\cdot)$ denotes the *base point* (i.e., the reference point defining the tangent space). Let the origin $o \in \mathcal{H}_c^d$ be defined as $o = (\sqrt{c}, 0, \dots, 0)$. Let $\|v\|_L = \sqrt{\langle v, v \rangle_L}$ (in the tangent space, this norm is real and non-negative). The exponential and logarithmic maps based at the origin o are then given by:

$$\exp_o(v) = \cosh\left(\frac{\|v\|_L}{\sqrt{c}}\right) o + \sqrt{c} \sinh\left(\frac{\|v\|_L}{\sqrt{c}}\right) \frac{v}{\|v\|_L}, \quad (2)$$

$$\log_o(x) = \frac{\operatorname{arccosh}\left(-\frac{\langle o, x \rangle_L}{c}\right)}{\left\|x + \frac{\langle o, x \rangle_L}{c} o\right\|_L} \left(x + \frac{\langle o, x \rangle_L}{c} o\right). \quad (3)$$

Base-point maps and parallel transport. The subscript in $\exp_x(\cdot)$ and $\log_x(\cdot)$ denotes the *base point* x that defines the tangent space $T_x \mathbb{H}_c^d$: $\exp_x : T_x \mathbb{H}_c^d \rightarrow \mathbb{H}_c^d$ and $\log_x : \mathbb{H}_c^d \rightarrow T_x \mathbb{H}_c^d$.

Parallel transport (PT). Parallel transport moves a tangent vector from one tangent space to another along the (unique) geodesic [3]. Formally, for a geodesic γ with $\gamma(0) = x$, $\gamma(1) = y$, PT is defined by the Levi-Civita connection:

$$\nabla_{\dot{\gamma}(t)} v(t) = 0, \quad v(0) = v_x, \quad \text{PT}_{x \rightarrow y}(v_x) = v(1),$$

which preserves the Riemannian inner product (lengths and angles).

In the Lorentz model $\mathcal{H}_c^d = \{x : \langle x, x \rangle_L = -c, x_0 > 0\}$ with metric $g_c^d(u, v) = \langle u, v \rangle_L$, a closed-form expression for PT along the geodesic from x to y is:

$$\text{PT}_{x \rightarrow y}(v) = v + \frac{\langle y, v \rangle_L}{c - \langle x, y \rangle_L} (x + y), \quad v \in T_x \mathbb{H}_c^d. \quad (4)$$

This mapping satisfies:

$$\text{PT}_{x \rightarrow y}(v) \in T_y \mathbb{H}_c^d, \quad \langle \text{PT}_{x \rightarrow y}(v_1), \text{PT}_{x \rightarrow y}(v_2) \rangle_L = \langle v_1, v_2 \rangle_L. \quad (5)$$

In the subsequent derivations and implementation, we set the curvature parameter $c = 1$. Following prior work [4, 25], we consistently use $o = (1, 0, \dots, 0)$ as the reference point and employ $\exp_o(\cdot)$ and $\log_o(\cdot)$ for transformations between \mathbb{H}^d and the tangent space $T_o \mathbb{H}^d$ when a fixed base point is sufficient; in the moving-base formulation, we instead use $\exp_x(\cdot)$, $\log_x(\cdot)$, and $\text{PT}_{x \rightarrow y}(\cdot)$ with dynamically changing base points.

4 The Proposed Model

4.1 Overview

As illustrated in Figure 2, the overall framework of our proposed GTR-Mamba consists of three integral components. We learn hyperbolic embeddings and relation-specific rotations jointly with the sequential model, and use them to form the trajectory input representation. Parallel to this, we employ a Euclidean Spatio-Temporal Channel that encodes geographical contexts using spherical multi-scale Random Fourier Features (RFF), while capturing temporal dynamics via multi-frequency sine-cosine encoding. Subsequently, the sequence representation is routed into the core GTR-Mamba Layer, where the internal State Space Model (SSM) is explicitly driven by the encoded Euclidean spatio-temporal signals. Finally, the next POI is predicted through a dual-path scoring mechanism that aggregates scores from both the hyperbolic manifold and the Euclidean tangent space.

4.2 Hyperbolic Rotational Alignment

Following prior research [11, 30], we optimize entity representations on the Lorentz manifold to capture static hierarchical and transitional relationships. We construct a multi-relational graph from historical check-ins, encompassing User-POI interactions, sequential POI transitions (within a 6-hour window), and their corresponding category and region transitions. To align diverse semantics, learnable isometric rotations $\text{Rot}(\cdot)$ are applied to source embeddings to better align them with targets while preserving

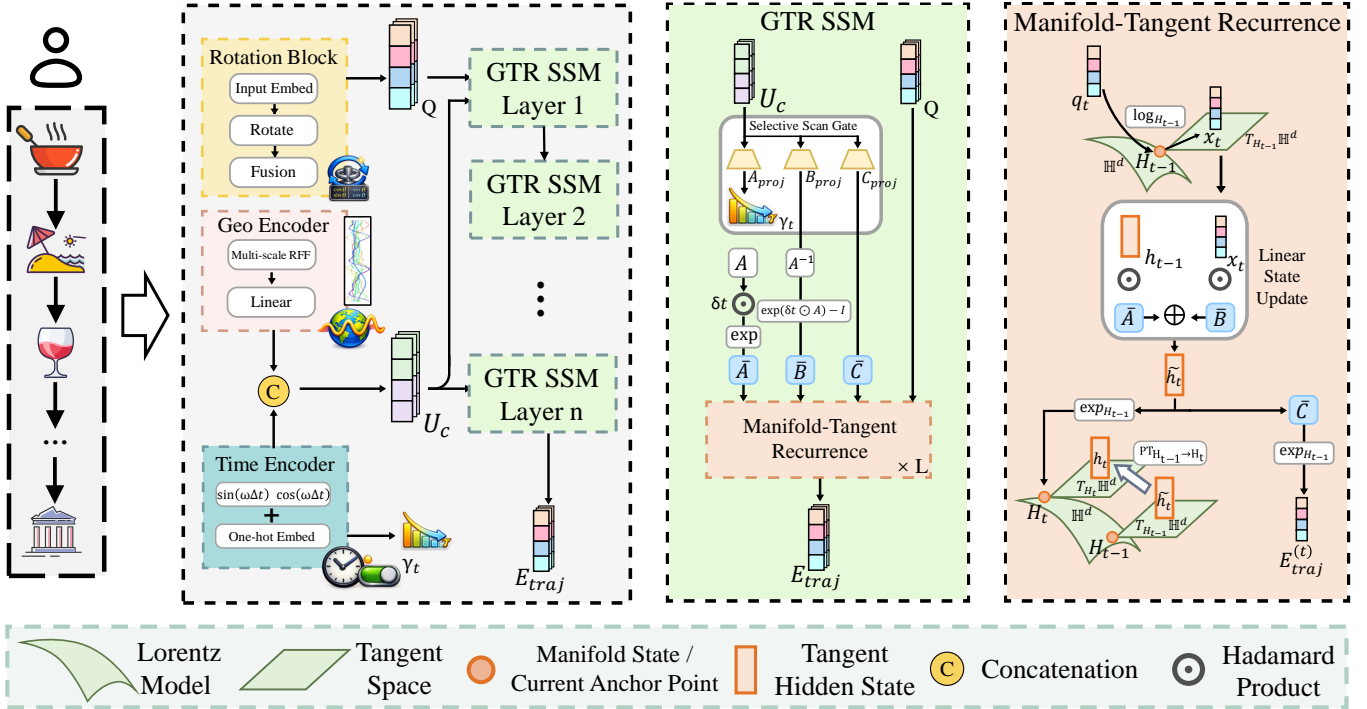


Figure 2: The overall architecture of GTR-Mamba. The framework comprises three key components: (1) *Hyperbolic Rotational Alignment* via rotation-based contrastive learning; (2) An exogenous *Spatio-Temporal Channel* encoding Euclidean contexts; and (3) The *GTR-Mamba Layer*, which routes state transitions to the tangent space using Parallel Transport (PT) while modulating SSM parameters via external context signals.

the Lorentzian inner product. The model is optimized using a contrastive loss that maximizes the similarity scores s_t (including positive sample score $s_{\text{pos},t}$ and negative sample score $s_{\text{neg},t}$) for observed edges across all types $t \in \{up, pp, cc, rr\}$:

$$\mathcal{L}_{\text{rot}} = - \sum_t \left(\sum \log \sigma(s_{\text{pos},t}) + \sum \log \sigma(-s_{\text{neg},t}) \right), \quad (6)$$

where $\sigma(\cdot)$ is the sigmoid function.

Given the hyperbolic embeddings $\mathbf{E}_p, \mathbf{E}_c, \mathbf{E}_u, \mathbf{E}_r$, we fuse these multi-modal representations via semantic composition in the tangent space. Specifically, we project each entity’s embedding onto the tangent space at the origin o using the logarithmic map and compute the sequence representation \mathbf{q}_t :

$$\mathbf{q}_t = \alpha_u \log_o(\mathbf{E}_u) + \alpha_p \log_o(\mathbf{E}_p) + \alpha_c \log_o(\mathbf{E}_c) + \alpha_r \log_o(\mathbf{E}_r), \quad (7)$$

where α are hyperparameters used to prioritize different semantic objectives. This composite vector is finally mapped back to the manifold to obtain the hyperbolic sequence representation $\mathbf{q}_t \in \mathbb{H}^d$. We then stack $\{\mathbf{q}_t\}_{t=1}^L$ to form the initialized trajectory $\mathbf{Q} = [\mathbf{q}_1, \dots, \mathbf{q}_L] \in \mathbb{H}^{L \times d}$ for subsequent sequence modeling.

4.3 Spatio-temporal Channel

While hyperbolic embeddings capture hierarchical semantics, they lack explicit awareness of linear spatio-temporal dynamics (e.g., continuous time intervals). Instead of forcing Euclidean spatio-temporal signals (e.g., time intervals, grid coordinates) into the

hyperbolic manifold—which risks geometric distortion and semantic misalignment—we encode them via an exogenous Euclidean channel to linearly modulate the SSM dynamics.

4.3.1 Geographic Embedding Module. Our geographical embedding module encodes latitude and longitude via multi-scale Random Fourier Features (RFF) to obtain a high-dimensional harmonic representation of spatial contexts.

First, we map latitude and longitude to unit vectors on a sphere. We then sample a multi-scale Gaussian frequency matrix and compute harmonic features by sine-cosine projections, yielding global multi-scale geographical features \mathbf{E}_{RFF} . Finally, a linear projection is applied to obtain the geographic embedding $\mathbf{E}_g \in \mathbb{R}^{L \times d_{\text{geo}}}$.

4.3.2 Temporal Feature Module. The temporal feature module is responsible for generating temporal representations and a decay factor, which are used to modulate the dynamic evolution of the SSM.

We first extract the time interval $\Delta t \in \mathbb{R}^{L \times 1}$, the day of the week (dow), and the hour of the day (hour) from the time series. These are then fused into a feature vector:

$$\mathbf{E}_t = \text{Concat}[\Delta t; \sin(\omega \Delta t); \cos(\omega \Delta t); \text{OH}(\text{dow}); \text{OH}(\text{hour})], \quad (8)$$

where $\omega \in \mathbb{R}^M$ denotes a vector of M logarithmically spaced frequencies, $\mathbf{E}_t \in \mathbb{R}^{L \times d_{\text{time}}}$, and $\text{OH}(\text{dow})$ and $\text{OH}(\text{hour})$ are 7-dimensional and 24-dimensional one-hot encodings, respectively. This design captures both the periodicity and long-term trends of temporal data.

The feature vector is then projected to a dimension of d_{time} , and a decay factor is computed via a gated mechanism:

$$\gamma_t = \sigma(\mathbf{E}_t \cdot \mathbf{w}_{\text{gate}}), \quad (9)$$

where $\gamma_t \in \mathbb{R}^{L \times 1}$ and $\mathbf{w}_{\text{gate}} \in \mathbb{R}^{d_{\text{time}}}$ is a learnable weight vector. This decay factor γ_t modulates the step size of the SSM, simulating the influence of time intervals on the trajectory dynamics. Let $\mathbf{u}_c = \text{Concat}[\mathbf{E}_g; \mathbf{E}_t]$ denote the combined Euclidean context feature.

4.4 GTR-Mamba Layer

To address the modeling challenges of sequence-encoded tasks, we adopt the Mamba framework [13]. Its selective scanning mechanism, enabled by dynamic step sizes and input gating, adaptively captures variations in temporal intervals and external spatiotemporal contexts. Furthermore, Mamba’s linear recursive computation facilitates efficient dynamic updates in a local tangent space, making it particularly suitable for trajectory modeling on non-Euclidean manifolds.

For enhanced stability and computational efficiency, we employ a fixed diagonal matrix:

$$\mathbf{A} = -\text{diag}(\log(2), \log(3), \dots, \log(d+1)). \quad (10)$$

This structure naturally accommodates the multi-time-scale characteristics of trajectory data, ranging from short-term frequent check-ins to long-term behavioral patterns. To address the lack of cross-channel mixing in the diagonal matrix \mathbf{A} , which lacks cross-channel coupling, we implement dynamic channel modulation on the input side through context-driven selective gating.

The step size δt is dynamically generated based on the Euclidean features \mathbf{u}_c :

$$\delta t = (A_{\text{proj}}(\mathbf{u}_c) \cdot \mathbf{W}_{dt} + \mathbf{b}_{dt}) \odot \gamma_t, \quad (11)$$

where $A_{\text{proj}}: \mathbb{R}^d \rightarrow \mathbb{R}^d$, $\mathbf{W}_{dt} \in \mathbb{R}^d$ is a learnable vector, $\mathbf{b}_{dt} \in \mathbb{R}^d$ is a learnable bias, and $\gamma_t \in \mathbb{R}^{L \times 1}$ is the decay factor obtained from the temporal encoding module.

Subsequently, we discretize the continuous SSM. The state transition matrix $\tilde{\mathbf{A}} \in \mathbb{R}^{L \times d}$ is:

$$\tilde{\mathbf{A}} = \exp(\delta t \odot \mathbf{A}), \quad (12)$$

and the input matrix $\tilde{\mathbf{B}} \in \mathbb{R}^{L \times d}$ is:

$$\tilde{\mathbf{B}} = (\exp(\delta t \odot \mathbf{A}) - \mathbf{I}) \odot \mathbf{A}^{-1}, \quad (13)$$

where \mathbf{I} is the identity matrix.

To inject the exogenous contextual conditions, the input matrix $\tilde{\mathbf{B}}$ is modulated by selective weights derived from the Euclidean context features:

$$\tilde{\mathbf{B}} \leftarrow \tilde{\mathbf{B}} \odot B_{\text{proj}}(\mathbf{u}_c), \quad (14)$$

where $B_{\text{proj}}: \mathbb{R}^d \rightarrow \mathbb{R}^d$. This element-wise multiplication allows each state dimension to independently determine its input strength based on the spatio-temporal context.

Prior research has demonstrated that tangent space approximation introduces distortion, and restricting operations to a fixed tangent space limits the model’s ability to leverage the rich information of the manifold [3, 62]. Inspired by Bose et al., our model incorporates Parallel Transport (PT) to enable selective scanning within a moving tangent space anchored at the current manifold state [3]. Parallel transport serves as the canonical generalization of

Euclidean translation to Riemannian manifolds. Given that the core recurrence of Mamba involves linear state transitions, PT provides the necessary geometric operator to transport updated hidden states between varying reference points while preserving the Riemannian metric structure.

Let $\mathbf{H}_{t-1} \in \mathbb{H}^d$ denote the manifold anchor at step $t-1$. We first map the current hyperbolic input $\mathbf{q}_t \in \mathbb{H}^d$ to the local tangent space at \mathbf{H}_{t-1} :

$$\mathbf{x}_t = \log_{\mathbf{H}_{t-1}}(\mathbf{q}_t) \in T_{\mathbf{H}_{t-1}}\mathbb{H}^d. \quad (15)$$

We maintain a tangent-space hidden state $\mathbf{h}_{t-1} \in T_{\mathbf{H}_{t-1}}\mathbb{H}^d$ and update it linearly in the same local tangent space:

$$\tilde{\mathbf{h}}_t = \tilde{\mathbf{A}}_t \odot \mathbf{h}_{t-1} + \tilde{\mathbf{B}}_t \odot \mathbf{x}_t. \quad (16)$$

Note that $\tilde{\mathbf{h}}_t$ resides in the tangent space of the previous anchor \mathbf{H}_{t-1} .

We then map the updated tangent vector $\tilde{\mathbf{h}}_t$ back to the manifold via the exponential map anchored at \mathbf{H}_{t-1} :

$$\mathbf{H}_t = \exp_{\mathbf{H}_{t-1}}(\tilde{\mathbf{h}}_t) \in \mathbb{H}^d. \quad (17)$$

Formally, the validity of the GTR mechanism is grounded in the differential geometric principle that linear operations are strictly local. While the SSM core performs efficient linear recurrence, it implicitly assumes a flat vector space structure. On a curved Lorentz manifold, however, the tangent spaces $T_{\mathbf{H}_{t-1}}\mathbb{H}^d$ and $T_{\mathbf{H}_t}\mathbb{H}^d$ are distinct vector spaces. Unlike in Euclidean space, where vectors can be trivially translated due to zero curvature, in hyperbolic space, the basis vectors of the tangent space undergo rotation as they move along the manifold—a phenomenon governed by the manifold’s non-zero curvature and holonomy. Consequently, directly reusing a hidden vector from the previous step without adjustment is mathematically ill-posed, as it ignores the geometric twisting of the coordinate system.

To rigorously bridge this gap, we employ the Levi-Civita Parallel Transport (PT) along the unique geodesic connecting the consecutive anchors \mathbf{H}_{t-1} and \mathbf{H}_t . This operator defines an isometric isomorphism between the disjoint tangent spaces, preserving the Riemannian metric properties (i.e., inner products, norms, and angles). Conceptually, this step acts as a discrete realization of *covariant transport*, explicitly rectifying the frame misalignment caused by the manifold’s curvature. By compensating for the geometric rotation, PT ensures that the historical state \mathbf{h}_{t-1} is faithfully translated into the new reference frame $T_{\mathbf{H}_t}\mathbb{H}^d$, maintaining the physical consistency of the sequence memory across recursive updates:

$$\mathbf{h}_t = \text{PT}_{\mathbf{H}_{t-1} \rightarrow \mathbf{H}_t}(\tilde{\mathbf{h}}_t) \in T_{\mathbf{H}_t}\mathbb{H}^d. \quad (18)$$

This transported vector \mathbf{h}_t effectively becomes the valid hidden state for the subsequent time step.

Then we introduce a context-driven C -projection. Specifically, for each time step we generate a vector $\mathbf{c}_t \in \mathbb{R}^d$ from the Euclidean spatio-temporal feature \mathbf{u}_c (time-step sliced), and apply an element-wise product along the state dimension to modulate the recurrent state:

$$\mathbf{c}_t = \sigma(C_{\text{proj}}(\mathbf{u}_c)) \in \mathbb{R}^d, \quad \mathbf{o}_t = \mathbf{c}_t \odot \tilde{\mathbf{h}}_t \in T_{\mathbf{H}_{t-1}}\mathbb{H}^d, \quad (19)$$

where $C_{\text{proj}} : \mathbb{R}^d \rightarrow \mathbb{R}^d$. The per-step trajectory embedding is obtained by mapping the readout vector back to the manifold:

$$\mathbf{E}_{\text{traj}}^{(t)} = \exp_{\mathbb{H}_{t-1}}(\mathbf{o}_t) \in \mathbb{H}^d. \quad (20)$$

By stacking the per-step embeddings over $t = 1, \dots, L$, we obtain $\mathbf{E}_{\text{traj}} = [\mathbf{E}_{\text{traj}}^{(1)}, \dots, \mathbf{E}_{\text{traj}}^{(L)}] \in \mathbb{H}^{L \times d}$.

Compared to a fixed-origin global linearization, the moving-base formulation performs local linearization along the trajectory and propagates memory with parallel transport, reducing accumulated distortion on long and irregular trajectories.

4.5 Prediction and Loss

Having encoded the user’s dynamic preference evolution into the trajectory embedding \mathbf{E}_{traj} , the final step is to predict the next likely visit. Our method also forecasts potential transitions between categories and regions to aid in the next location prediction. In other words, we integrate the results from these multiple tasks to formulate the final recommendation. Here, we use POI prediction as an illustrative example; the prediction process for the other tasks is analogous. The total prediction loss is the sum of these individual losses:

$$\mathcal{L}_{\text{all}} = \mathcal{L}_{\text{poi}} + \mathcal{L}_{\text{cat}} + \mathcal{L}_{\text{reg}} + \mathcal{L}_{\text{rot}}. \quad (21)$$

Our prediction component performs scoring from both the hyperbolic and tangent spaces.

To capture the geometric relationships between embeddings, we compute the squared Lorentz distance, $d_L^2(\cdot, \cdot)$, on the manifold between the GTR-Mamba output trajectory embedding, \mathbf{E}_{traj} , and all candidate entities (POIs, categories, or regions). The similarity score is defined as:

$$s_{\text{hyperbolic}} = -\frac{\sqrt{d_L^2(\mathbf{E}_{\text{traj}}, \mathbf{p})}}{\tau}, \quad (22)$$

where τ is a learnable temperature parameter. For POI prediction, \mathbf{p} represents the embeddings of all POIs $\mathbf{E}_{\mathcal{P}} \in \mathbb{H}^{|\mathcal{P}| \times d}$. This distance-based score leverages the geometric properties of the Lorentz manifold by directly comparing embeddings in the hyperbolic space, which is well-suited for hierarchical data.

Concurrently, the tangent vector of the trajectory is decoded through a linear layer to produce logit scores for the candidate entities:

$$s_{\text{tangent}} = \text{Linear}(\log_{\mathbf{o}}(\mathbf{E}_{\text{traj}})). \quad (23)$$

This provides a direct classification prediction that captures the linear patterns within the tangent space.

To balance the geometric scores and the linear predictions, we introduce a learnable mixing parameter β . The final prediction score is a weighted combination:

$$s = \beta \cdot s_{\text{tangent}} + (1 - \beta) \cdot s_{\text{hyperbolic}}. \quad (24)$$

This formulation combines the hierarchical expressive power of hyperbolic distance with the flexibility of a linear decoder, adaptively adjusting the weights of the two components via the parameter β .

For the POI, category, and region prediction tasks, we employ the cross-entropy loss, yielding the respective losses \mathcal{L}_{poi} , \mathcal{L}_{cat} , and \mathcal{L}_{reg} .

5 Experiments and Results

5.1 Dataset

We evaluate our proposed model on three datasets collected from two real-world check-in platforms: Foursquare [50] and Gowalla [57]. The Foursquare dataset includes two subsets, which are collected from New York City (NYC) in the USA and Tokyo (TKY) in Japan. The Gowalla dataset includes one subset collected from California and Nevada (CA). Their detailed statistics are in Table 1. The density is calculated as the total number of visits divided by (number of users \times number of POIs), which is used to reflect the sparsity level between users and POIs. Following prior work [36], we remove POIs with fewer than five check-ins, segment each user’s trajectory into sequences of length 3–101, and split the data into training, validation, and test sets in an 8:1:1 ratio.

Table 1: Statistics of the evaluated datasets.

	User	POI	Category	Traj	Check-in	Density
NYC	1,047	4,980	318	13,955	101,760	0.016
TKY	2,281	7,832	290	65,914	403,148	0.018
CA	3,956	9,689	296	42,982	221,717	0.005

5.2 Experiment Setting

In our experiments, the curvature parameter, c , of the hyperbolic space was set to 1. We configured the model with the following default hyperparameters: a batch size of 128, a learning rate of 0.001, and a training duration of 50 epochs. Weights α_u , α_p , α_c and α_r were set to 0.5, 0.3, 0.1 and 0.1 respectively. The entire geographical area was partitioned into 40 regions. The embedding dimension, d , was set to 64, with the geographical and temporal encoding dimensions set to 16 and 24, respectively. For the auxiliary relational alignment loss, we used 5 negative samples per positive instance. The Mamba architecture consisted of 2 layers.

We evaluated the recommendation performance using Top-k Normalized Discounted Cumulative Gain (NDCG@k) and Mean Reciprocal Rank (MRR). We report results for $k \in \{1, 5, 10\}$. The model is implemented in PyTorch and executed on an NVIDIA GeForce RTX 4090 GPU.

5.3 Baseline Model

We compare GTR-Mamba against 12 baselines, categorized into Euclidean and Hyperbolic methods. **Euclidean-based methods** include: **LSTM** [15] and **PLSPL** [45], which utilize RNNs and attention for sequential preference learning; **GETNext** [54], which incorporates global trajectory flow maps; **AGRAN** [44], employing adaptive graph structure learning; **MCLP** [37], utilizing topic modeling and multi-head attention; **GeoMamba** [6], Leveraging Mamba’s linear complexity with a hierarchical geography encoder for efficient sequential modeling and **GeoMamba** [32], extending SSMs with a GaPPO operator to model multi-granular spatio-temporal transitions; **Hyperbolic-based methods** include: **HME** [11], embedding check-ins into a Poincaré ball; **HMST** [30], employing hyperbolic rotations to jointly model hierarchical structures and multi-semantic transitions; **HVGAE** [25], integrating a Hyperbolic

Table 2: Overall performance comparison with baseline models on three datasets. Top-1, Top-2.

Method	NYC				TKY				CA			
	ND@1	ND@5	ND@10	MRR	ND@1	ND@5	ND@10	MRR	ND@1	ND@5	ND@10	MRR
LSTM	0.1306	0.2336	0.2585	0.2259	0.1110	0.2233	0.2496	0.1952	0.0864	0.1459	0.1711	0.1554
PLSPL	0.1601	0.3048	0.3336	0.2849	0.1495	0.2831	0.3143	0.2642	0.1084	0.1759	0.2029	0.1678
HME	0.1619	0.2806	0.3226	0.2787	0.1535	0.2637	0.2924	0.2366	0.1181	0.1886	0.2232	0.1945
GETNext	0.2244	0.3736	0.4046	0.3472	0.1767	0.3072	0.3297	0.2934	0.1342	0.2188	0.2468	0.2121
AGRAN	0.2202	0.3638	0.3792	0.3343	0.1755	0.2989	0.3261	0.2879	0.1329	0.2121	0.2331	0.2043
MCLP	<u>0.2404</u>	0.3674	0.3973	0.3507	0.1662	0.3110	0.3415	0.3199	0.1324	0.1914	0.2121	0.1895
GeoMamba'24	0.1988	0.3392	0.3506	0.3246	0.1851	0.2953	0.3205	0.2858	0.1256	0.2029	0.2215	0.1962
GeoMamba'25	0.2377	<u>0.3786</u>	0.4012	<u>0.3566</u>	<u>0.2157</u>	<u>0.3402</u>	0.3686	0.3209	0.1388	0.2485	0.2754	0.2373
HMamba _{full}	0.2204	0.3679	0.4031	0.3465	0.1828	0.3341	0.3673	0.3127	0.1366	<u>0.2501</u>	<u>0.2792</u>	<u>0.2421</u>
HMamba _{half}	0.1896	0.3453	0.3767	0.3222	0.1945	0.3295	0.3603	0.3118	<u>0.1423</u>	0.2381	0.2648	0.2317
HMST	0.2138	0.3747	<u>0.4063</u>	0.3482	0.1925	0.3325	<u>0.3690</u>	<u>0.3257</u>	0.1356	0.2325	0.2680	0.2300
HVGAE	0.2271	0.3651	0.3982	0.3470	0.1977	0.3167	0.3455	0.3180	0.1391	0.2325	0.2658	0.2367
GTR-Mamba	0.2473	0.3949	0.4266	0.3709	0.2502	0.3757	0.4045	0.3596	0.1610	0.2627	0.2865	0.2548
<i>improv.</i>	↑+2.87%	↑+4.31%	↑+5.00%	↑+3.93%	↑+15.99%	↑+10.44%	↑+9.62%	↑+10.41%	↑+13.14%	↑+5.04%	↑+2.61%	↑+5.25%

GCN and Variational Graph Auto-Encoder with Rotary Position Mamba to capture hierarchical and sequential POI relationships; and **HMamba** [61], combining Mamba’s efficiency with hyperbolic geometry. We evaluate both the *Full* version (curvature-aware state spaces) and the *Half* version (simplified implementation). As HMamba was originally designed for standard sequential recommendation, we adapted it for POI tasks by incorporating temporal and geographical coordinate encoders.

To distinguish between the two identically named GeoMamba models, we append their year of publication. The two variants of HMamba are differentiated by the subscripts "full" and "half," respectively. Furthermore, as HMamba was originally designed for sequential recommendation, we have adapted it for our POI recommendation task to ensure a fairer comparison by incorporating encodings for temporal granularity and geographical coordinates to integrate spatio-temporal information.

5.4 Performance Comparison With Baselines

We first compare our model with 12 baseline models (Table 2). Our model consistently outperforms all baselines on the NYC and TKY (Foursquare) and CA (Gowalla) datasets. Improvements range from 2.61% to 15.99% in NDCG and 3.93% to 10.41% in MRR, demonstrating robustness in capturing spatio-temporal patterns.

Among baselines, Transformer-based approaches (GETNext and MCLP) surpass traditional models (LSTM, PLSPL) via multi-head attention mechanisms that capture complex sequential dependencies. AGRAN improves upon traditional GCNs through adaptive graph structures, while GeoMamba balances accuracy and efficiency using geographical encoding and Mamba’s sequential updating. However, these Euclidean-based models are constrained. In contrast, our model operates in hyperbolic space to comprehensively capture hierarchical patterns, leveraging Mamba for efficient, stable updates.

Secondly, our method significantly outperforms other hyperbolic

Table 3: Performance comparison of model variants.

Model	NYC			CA		
	ND@1	ND@5	MRR	ND@1	ND@5	MRR
w/o SSM (−)	0.1965	0.2928	0.2687	0.1236	0.2184	0.2027
w/o HE (−)	0.2143	0.3076	0.2916	0.1398	0.2464	0.2355
w/o HB (−)	0.2308	0.3789	0.3497	0.1432	0.2387	0.2371
w/o STC (−)	0.2374	0.3702	0.3544	0.1457	0.2406	0.2365
Fixed-Base (−)	0.2394	0.3811	0.3610	0.1508	0.2434	0.2353
Full model	0.2473	0.3949	0.3709	0.1610	0.2627	0.2548

approaches. HME is limited to node embeddings, while HVGAE and HMST model relationships better but lack powerful sequential update mechanisms. HMamba performs well but suffers computational overhead from direct manifold updates and lacks context handling. Conversely, our model’s geometry-to-tangent-space pathway ensures stable computation, and our novel exogenously-driven SSM provides higher accuracy in complex scenarios. Overall, our hyperbolic Mamba approach outperforms all baselines across the three datasets.

5.5 Ablation Study

We conducted a comprehensive ablation study to validate the effectiveness of the individual components within our proposed model. Specifically, we designed the following ablation settings:

- w/o SSM (without State Space Model): This variant removes the geometry-to-tangent-space routing Mamba layer.

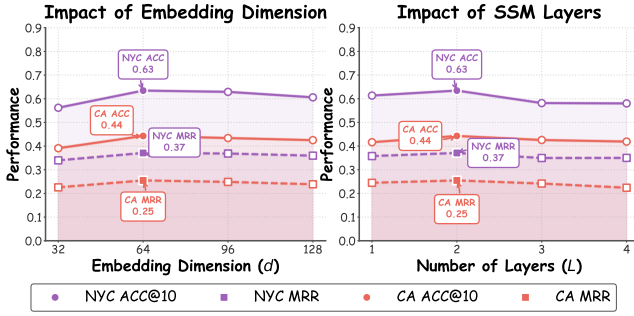


Figure 3: Performance w.r.t. different embedding dimensions and SSM layers

- w/o HE (without Hyperbolic Embedding): This version removes the initial hyperbolic embeddings that are learned with rotation.
- w/o HB (without Hyperbolic space): This variant implements the GTR-Mamba framework entirely in Euclidean space.
- w/o STC (without Spatio-Temporal Channel): This variant removes the spatio-temporal encoding channel.
- Fixed-Base: This variant performs all updates in a single global tangent space.

The ablation study results are reported in Table 3, presenting the ND@1, ND@5, and MRR metrics. Using the complete GTR-Mamba model as the baseline, we derive the following observations. The most significant performance degradation across all metrics is observed when the entire Mamba sequence modeling module is removed (w/o SSM), underscoring the critical role of dynamic relational modeling in user trajectories for personalized POI recommendation. The second most impactful variant is the one without initialized embeddings (w/o HE), highlighting the importance of rotation-based modeling for capturing complex semantic relationships. The variant excluding hyperbolic space (w/o HB) also exhibits a notable decline in all three metrics, as Euclidean space fails to effectively capture latent hierarchical structures, demonstrating the advantage of hyperbolic geometry. The variant without Euclidean spatiotemporal information (w/o STC) indicates that Euclidean encodings provide complementary support to the hyperbolic model. Removing Parallel Transport (Fixed-Base) leads to a decline in all metrics, suggesting that the PT mechanism effectively mitigates the distortion caused by tangent space approximation.

5.6 Sensitivity Analysis

We analyze the impact of key hyperparameters on GTR-Mamba, specifically the embedding dimension and the number of SSM layers, with results summarized in Figure 3. Crucially, since the tangent space coordinates of hyperbolic embeddings serve directly as state vectors for the Selective SSM, the SSM state dimension is inherently coupled with the node embedding dimension.

5.6.1 Embedding Dimension. We evaluate embedding dimensions $d \in \{32, 64, 96, 128\}$ on the NYC and CA datasets. Note that for this analysis, we report ACC@10 and MRR, distinct from the NDCG metrics used in the main experiments. As shown in Figure 3 (Left),

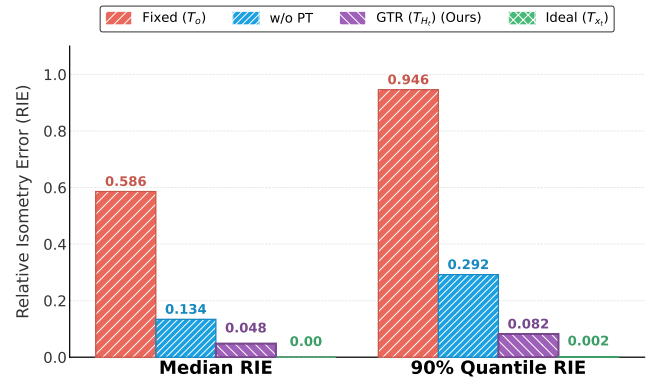


Figure 4: Median and 90% Quantile of RIE. GTR (purple) minimizes distortion. w/o PT (blue) underperforms GTR due to geometric misalignment, while Fixed (red) suffers from collapse.

Table 4: Time complexity analysis of GTR-Mamba components.

Component	Time Complexity
Hyperbolic Representation Learning	$O(\mathcal{E}_s \cdot (K+1) \cdot d)$
Spatio-temporal Channel (RFF)	$O(L \cdot m + L \cdot d)$
GTR-Mamba Layer	$O(n \cdot L \cdot d^2)$

performance peaks at $d = 64$ and degrades with higher dimensions. Consequently, we set $d = 64$ for all experiments.

5.6.2 Number of SSM Layers. We examine the effect of model depth by varying the number of SSM layers $L \in \{1, 2, 3, 4\}$. Figure 3 (Right) indicates that while deeper models capture higher-order spatiotemporal interactions, performance plateaus beyond $L = 2$ while computational costs (time and memory) rise significantly. We therefore adopt a 2-layer configuration to balance efficiency and accuracy.

5.7 Geometric Distortion Analysis

To quantify the approximation error, we use the *Relative Isometry Error* (RIE). For consecutive POIs (x_t, x_{t+1}) , RIE is defined as $|\hat{d} - d_{\mathbb{H}}| / (d_{\mathbb{H}} + \epsilon)$, where $d_{\mathbb{H}}$ is the geodesic distance and \hat{d} is the tangent space distance. We compare four settings: (1) **Fixed** (T_o): projecting to the origin; (2) **w/o PT**: moving base without parallel transport; (3) **GTR** (T_{H_t}): our full model anchored at H_t ; and (4) **Ideal** (T_{x_t}): the theoretical lower bound.

Figure 4 reports the Median and 90% Quantile of RIE on the NYC dataset. The **Fixed** strategy (red) shows severe distortion, confirming that projecting boundary nodes to a fixed origin induces severe metric distortion, especially for points far from the origin. The **w/o PT** variant (blue) reduces error but still lags behind GTR, indicating that moving the base without geometric calibration causes hidden state misalignment. Crucially, **GTR** (purple) achieves minimal error (median 0.048), substantially closer to the **Ideal** bound (green). This

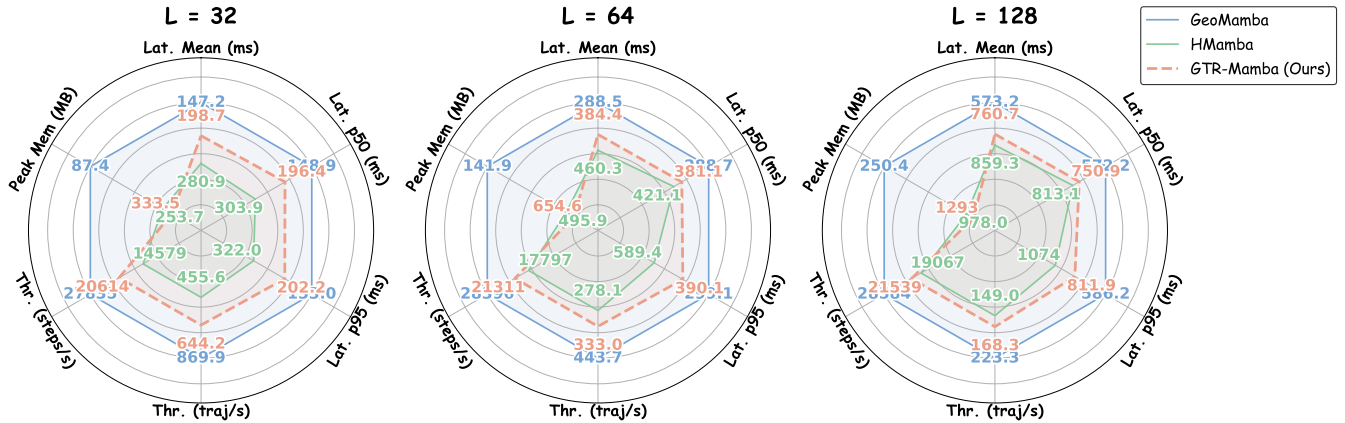


Figure 5: Efficiency comparison: End-to-end inference latency (ms/batch), throughput (steps/s) and peak GPU memory (MB). GTR-Mamba (red) is slower than Euclidean GeoMamba variants (blue) due to necessary hyperbolic primitives, but remains faster than fully hyperbolic HMamba (green) by routing the scan core to the tangent space and avoiding heavy manifold recurrences.

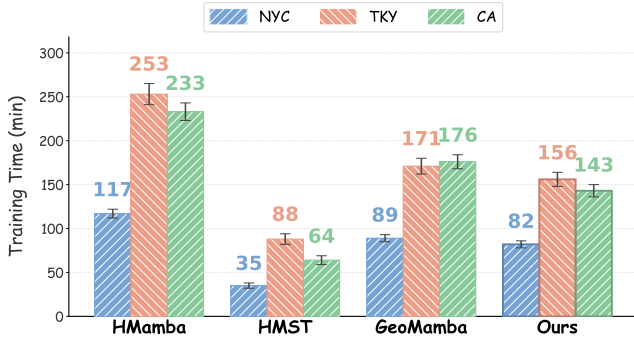


Figure 6: Training efficiency analysis. The curves depict the wall-clock time required for each model to reach 95% of its optimal MRR convergence. GTR-Mamba achieves a superior balance, converging faster than complex methods while reaching higher performance ceilings.

verifies that Parallel Transport is essential for maintaining metric fidelity in a dynamic tangent space.

5.8 Efficiency

Our GTR-Mamba consists of three components: (i) hyperbolic representation learning on the Lorentz manifold, (ii) a Euclidean spatio-temporal channel, and (iii) the core GTR-Mamba layer with tangent-space selective scanning. We evaluate efficiency from three aspects: asymptotic complexity, end-to-end training time-to-quality, and end-to-end inference latency/throughput.

5.8.1 Asymptotic complexity. We analyze the asymptotic time complexity of each component below.

Variable descriptions.

- **Hyperbolic Representation Learning:** $|V|$ is the number of entities (users, POIs, categories, regions), d is the embedding dimension, $|\mathcal{E}_s|$ is the number of sampled positive edges used to compute \mathcal{L}_{rot} (e.g., per epoch or per

mini-batch), and K is the number of negative samples per positive edge.

- **Spatio-temporal Channel:** L is the sequence length, m is the total number of Random Fourier Features (including multi-scale bases), and d is the model dimension after projection.
- **GTR-Mamba Layer:** n is the number of stacked layers. The $O(d^2)$ term comes from per-position linear projections for context-driven parameterization (e.g., $A_{\text{proj}}, B_{\text{proj}}, C_{\text{proj}}$). The $O(d)$ term corresponds to the linear-time selective scan with diagonal A , plus Lorentz manifold primitives (log/exp maps, inner products, and closed-form PT), each costing $O(d)$ per position. We treat the SSM state size and Euclidean context width as $O(d)$ in our implementation, so the overall per-layer cost remains quadratic in d .

5.8.2 End-to-end inference latency and throughput. We benchmark end-to-end inference on a single GPU with FP16 AMP. Unless otherwise stated, we use batch size $B=128$, warmup 20 iterations, and report statistics over 200 timed iterations. Latency is measured per batch (ms) and we report mean/p50/p95. Throughput is reported in trajectories/s and steps/s, and peak GPU memory is reported in MB.

As shown in Figure 5, GTR-Mamba sits between Euclidean and fully-hyperbolic SSM baselines in end-to-end efficiency. Compared to GeoMamba [32], GTR-Mamba incurs a moderate constant-factor overhead (mean latency 1.33–1.35 \times , throughput 0.74–0.75 \times), attributable to manifold-related operations and geometric scoring. Meanwhile, GTR-Mamba remains faster than HMamba across sequence lengths (throughput 1.13–1.41 \times higher), while using moderately higher peak memory ($\sim 1.31\times$).

5.8.3 Training time-to-quality. Additionally, we compare the training time of our model against baseline models across three datasets. For a fair comparison, we measure the total wall-clock time required for each model to reach a fixed quality threshold under identical experimental conditions. Following prior practice, we define convergence as achieving 95% of the optimal MRR of each method. As shown in Figure 6, our model achieves a favorable balance between

time efficiency and ranking performance. GeoMamba referenced here corresponds to GeoMamba'25 [32], as distinguished from GeoMamba'24 [6] in baseline comparisons.

6 Conclusion

In this paper, we propose GTR-Mamba, a novel framework that effectively reconciles the representational superiority of hyperbolic geometry with the computational efficiency of Selective State Space Models for next POI recommendation. GTR-Mamba executes high-order sequence modeling within the computationally efficient Euclidean tangent space, while employing a Parallel Transport (PT) mechanism to dynamically align tangent spaces across varying reference points. This effectively mitigates the distortion arising from tangent space approximation and preserves geometric consistency. This process is coordinated by an exogenous spatio-temporal channel, enabling the internal dynamics of the SSM to be explicitly driven by irregular time intervals and geographical contexts. Extensive empirical evaluations on three real-world LBSN datasets demonstrate that GTR-Mamba consistently outperforms state-of-the-art baselines, including advanced graph-based and Mamba-based approaches. Our ablation studies and efficiency analysis further validate that the framework achieves a superior trade-off between recommendation accuracy and training scalability. For future work, we plan to extend this geometry-aware mechanism to other Riemannian manifolds, such as spherical or product spaces.

References

- [1] Ramesh Baral, SS Iyengar, Tao Li, and N Balakrishnan. 2018. Close: Contextualized location sequence recommender. In *Proceedings of the 12th ACM conference on recommender systems*. 470–474.
- [2] Ramesh Baral, Tao Li, and XiaoLong Zhu. 2018. CAPS: Context aware personalized POI sequence recommender system. *arXiv preprint arXiv:1803.01245* (2018).
- [3] Joey Bose, Ariella Smofsky, Renjie Liao, Prakash Panangaden, and Will Hamilton. 2020. Latent variable modelling with hyperbolic normalizing flows. In *International conference on machine learning*. PMLR, 1045–1055.
- [4] Ines Chami, Zitao Ying, Christopher Ré, and Jure Leskovec. 2019. Hyperbolic graph convolutional neural networks. *Advances in neural information processing systems* 32 (2019).
- [5] Jing Chen, Wenjun Jiang, Jie Wu, Kenli Li, and Keqin Li. 2023. Dynamic personalized POI sequence recommendation with fine-grained contexts. *ACM transactions on internet technology* 23, 2 (2023), 1–28.
- [6] Jiubing Chen, Haoyu Wang, and Jianxin Shang. 2024. GeoMamba: Towards Efficient Geography-aware Sequential POI Recommendation. *IEEE Access* (2024).
- [7] Yankai Chen, Menglin Yang, Yingxue Zhang, Mengchen Zhao, Ziqiao Meng, Jianye Hao, and Irwin King. 2022. Modeling scale-free graphs with hyperbolic geometry for knowledge-aware recommendation. In *Proceedings of the fifteenth ACM international conference on web search and data mining*. 94–102.
- [8] Yuntao Du, Xinjun Zhu, Lu Chen, Baihua Zheng, and Yunjun Gao. 2022. HAKG: Hierarchy-aware knowledge gated network for recommendation. In *Proceedings of the 45th international ACM SIGIR conference on Research and development in Information Retrieval*. 1390–1400.
- [9] Chenghua Duan, Wei Fan, Wei Zhou, Hu Liu, and Junhao Wen. 2023. Clsprec: Contrastive learning of long and short-term preferences for next poi recommendation. In *Proceedings of the 32nd acm international conference on information and knowledge management*. 473–482.
- [10] Jie Feng, Yong Li, Chao Zhang, Funing Sun, Fanchao Meng, Ang Guo, and Depeng Jin. 2018. Deepmove: Predicting human mobility with attentional recurrent networks. In *Proceedings of the 2018 world wide web conference*. 1459–1468.
- [11] Shanshan Feng, Lucas Vinh Tran, Gao Cong, Lisi Chen, Jing Li, and Fan Li. 2020. Hme: A hyperbolic metric embedding approach for next-poi recommendation. In *Proceedings of the 43rd International ACM SIGIR Conference on research and development in information retrieval*. 1429–1438.
- [12] Octavian Ganea, Gary Bécigneul, and Thomas Hofmann. 2018. Hyperbolic neural networks. *Advances in neural information processing systems* 31 (2018).
- [13] Albert Gu and Tri Dao. 2024. Mamba: Linear-time sequence modeling with selective state spaces. In *First Conference on Language Modeling*.
- [14] Naicheng Guo, Xiaolei Liu, Shaoshuai Li, Mingming Ha, Qiongxi Ma, Binfeng Wang, Yunan Zhao, Linxun Chen, and Xiaobo Guo. 2023. Hyperbolic contrastive graph representation learning for session-based recommendation. *IEEE Transactions on Knowledge and Data Engineering* (2023).
- [15] Sepp Hochreiter and Jürgen Schmidhuber. 1997. Long short-term memory. *Neural computation* 9, 8 (1997), 1735–1780.
- [16] Tianhao Huang, Xuan Pan, Xiangrui Cai, Ying Zhang, and Xiaojie Yuan. 2024. Learning time slot preferences via mobility tree for next poi recommendation. In *Proceedings of the AAAI Conference on Artificial Intelligence*, Vol. 38. 8535–8543.
- [17] Wei Jiang, Yongquan Fan, Jing Tang, Xianyong Li, Yajun Du, and Xiaomin Wang. 2026. Hierarchical long and short-term preference modeling with denoising Mamba for sequential recommendation. *Information Processing & Management* 63, 2 (2026), 104425.
- [18] Marc Law, Renjie Liao, Jake Snell, and Richard Zemel. 2019. Lorentzian distance learning for hyperbolic representations. In *International Conference on Machine Learning*. PMLR, 3672–3681.
- [19] Anchen Li, Bo Yang, Huan Huo, Hongxu Chen, Guangdong Xu, and Zhen Wang. 2022. Hyperbolic neural collaborative recommender. *IEEE Transactions on Knowledge and Data Engineering* 35, 9 (2022), 9114–9127.
- [20] Zeyu Li, Wei Cheng, Haiqi Xiao, Wenchao Yu, Haifeng Chen, and Wei Wang. 2021. You are what and where you are: Graph enhanced attention network for explainable poi recommendation. In *Proceedings of the 30th ACM International conference on information & knowledge management*. 3945–3954.
- [21] Defu Lian, Yongji Wu, Yong Ge, Xing Xie, and Enhong Chen. 2020. Geography-aware sequential location recommendation. In *Proceedings of the 26th ACM SIGKDD international conference on knowledge discovery & data mining*. 2009–2019.
- [22] Nicholas Lim, Bryan Hooi, See-Kiong Ng, Yong Liang Goh, Renrong Weng, and Rui Tan. 2022. Hierarchical multi-task graph recurrent network for next poi recommendation. In *Proceedings of the 45th international ACM SIGIR conference on Research and development in Information Retrieval*. 1133–1143.
- [23] Bin Liu, Chunyang Wang, Xuelian Liu, Guan Xi, Ge Zhang, Ziteng Yao, and Mengxue Dong. 2025. Hybrid-Emba3D: Geometry-Aware and Cross-Path Feature Hybrid Enhanced State Space Model for Point Cloud Classification. *arXiv e-prints* (2025), arXiv-2505.
- [24] Qiang Liu, Shu Wu, Liang Wang, and Tieniu Tan. 2016. Predicting the next location: A recurrent model with spatial and temporal contexts. In *Proceedings of the AAAI conference on artificial intelligence*, Vol. 30.
- [25] Yuwen Liu, Lianyong Qi, Xingyuan Mao, Weiming Liu, Fan Wang, Xiaolong Xu, Xuyun Zhang, Wanchun Dou, Xiaokang Zhou, and Amin Beheshti. 2025. Hyperbolic Variational Graph Auto-Encoder for Next POI Recommendation. In *Proceedings of the ACM on Web Conference 2025*. 3267–3275.
- [26] Yi-Shu Lu and Jiun-Long Huang. 2020. GLR: A graph-based latent representation model for successive POI recommendation. *Future Generation Computer Systems* 102 (2020), 230–244.
- [27] Yingtao Luo, Qiang Liu, and Zhaocheng Liu. 2021. Stan: Spatio-temporal attention network for next location recommendation. In *Proceedings of the web conference 2021*. 2177–2185.
- [28] Sarang Patil, Ashish Parmanand Pandey, Ioannis Koutis, and Mengjia Xu. 2025. Hierarchical Mamba Meets Hyperbolic Geometry: A New Paradigm for Structured Language Embeddings. *arXiv preprint arXiv:2505.18973* (2025).
- [29] Wei Peng, Tuomas Varanka, Abdelrahman Mostafa, Henglin Shi, and Guoying Zhao. 2021. Hyperbolic deep neural networks: A survey. *IEEE Transactions on pattern analysis and machine intelligence* 44, 12 (2021), 10023–10044.
- [30] Hongliang Qiao, Shanshan Feng, Min Zhou, WenTao Li, and Fan Li. 2025. Hyperbolic Multi-semantic Transition for Next POI Recommendation. In *Companion Proceedings of the ACM on Web Conference 2025*. 1830–1837.
- [31] Yifang Qin, Yifan Wang, Fang Sun, Wei Ju, Xuyang Hou, Zhe Wang, Jia Cheng, Jun Lei, and Ming Zhang. 2023. DisenPOI: Disentangling sequential and geographical influence for point-of-interest recommendation. In *Proceedings of the sixteenth ACM international conference on web search and data mining*. 508–516.
- [32] Yifang Qin, Jiakuan Xie, Zhiping Xiao, and Ming Zhang. 2025. GeoMamba: Towards Multi-granular POI Recommendation with Geographical State Space Model. In *Proceedings of the AAAI Conference on Artificial Intelligence*, Vol. 39. 12479–12487.
- [33] Pablo Sánchez and Alejandro Bellogín. 2022. Point-of-interest recommender systems based on location-based social networks: a survey from an experimental perspective. *ACM Computing Surveys (CSUR)* 54, 11s (2022), 1–37.
- [34] Ryotaro Shimizu, Yu Wang, Masanari Kimura, Yuki Hirakawa, Takashi Wada, Yuki Saito, and Julian McAuley. 2024. A fashion item recommendation model in hyperbolic space. In *Proceedings of the IEEE/CVF Conference on Computer Vision and Pattern Recognition*. 8377–8383.
- [35] Jianing Sun, Zhaoyue Cheng, Saba Zuberi, Felipe Pérez, and Maksims Volkovs. 2021. Hgcf: Hyperbolic graph convolution networks for collaborative filtering. In *Proceedings of the web conference 2021*. 593–601.
- [36] Ke Sun, Tiejun Qian, Tong Chen, Yile Liang, Quoc Viet Hung Nguyen, and Hongzhi Yin. 2020. Where to go next: Modeling long-and short-term user preferences for point-of-interest recommendation. In *Proceedings of the AAAI*

- conference on artificial intelligence*, Vol. 34. 214–221.
- [37] Tianao Sun, Ke Fu, Weiming Huang, Kai Zhao, Yongshun Gong, and Meng Chen. 2024. Going where, by whom, and at what time: Next location prediction considering user preference and temporal regularity. In *Proceedings of the 30th ACM SIGKDD Conference on Knowledge Discovery and Data Mining*. 2784–2793.
- [38] Dongjie Wang, Pengyang Wang, Kumpeng Liu, Yuanchun Zhou, Charles E Hughes, and Yanjie Fu. 2021. Reinforced imitative graph representation learning for mobile user profiling: An adversarial training perspective. In *Proceedings of the AAAI Conference on Artificial Intelligence*, Vol. 35. 4410–4417.
- [39] Hao Wang, Defu Lian, Hanghang Tong, Qi Liu, Zhenya Huang, and Enhong Chen. 2021. Hypersorec: Exploiting hyperbolic user and item representations with multiple aspects for social-aware recommendation. *ACM Transactions on Information Systems (TOIS)* 40, 2 (2021), 1–28.
- [40] Mu-Fan Wang, Yi-Shu Lu, and Jiun-Long Huang. 2019. SPENT: A successive POI recommendation method using similarity-based POI embedding and recurrent neural network with temporal influence. In *2019 IEEE International Conference on Big Data and Smart Computing (BigComp)*. IEEE, 1–8.
- [41] Shicheng Wang, Shu Guo, Lihong Wang, Tingwen Liu, and Hongbo Xu. 2023. Hdnr: A hyperbolic-based debiased approach for personalized news recommendation. In *Proceedings of the 46th International ACM SIGIR Conference on Research and Development in Information Retrieval*. 259–268.
- [42] Shoujin Wang, Liang Hu, Yan Wang, Longbing Cao, Quan Z Sheng, and Mehmet Orgun. 2019. Sequential recommender systems: challenges, progress and prospects. *arXiv preprint arXiv:2001.04830* (2019).
- [43] Zhaobo Wang, Yanmin Zhu, Haobing Liu, and Chunyang Wang. 2022. Learning graph-based disentangled representations for next POI recommendation. In *Proceedings of the 45th international ACM SIGIR conference on research and development in information retrieval*. 1154–1163.
- [44] Zhaobo Wang, Yanmin Zhu, Chunyang Wang, Wenzhe Ma, Bo Li, and Jiadi Yu. 2023. Adaptive graph representation learning for next POI recommendation. In *Proceedings of the 46th international ACM SIGIR conference on research and development in information retrieval*. 393–402.
- [45] Yuxia Wu, Ke Li, Guoshuai Zhao, and Xueming Qian. 2020. Personalized long-and short-term preference learning for next POI recommendation. *IEEE Transactions on Knowledge and Data Engineering* 34, 4 (2020), 1944–1957.
- [46] Jiayi Xie and Zhenzhong Chen. 2023. Hierarchical transformer with spatio-temporal context aggregation for next point-of-interest recommendation. *ACM Transactions on Information Systems* 42, 2 (2023), 1–30.
- [47] Xiaohang Xu, Toyotaro Suzumura, Jiawei Yong, Masatoshi Hanai, Chuang Yang, Hiroki Kanazashi, Renhe Jiang, and Shintaro Fukushima. 2023. Revisiting mobility modeling with graph: A graph transformer model for next point-of-interest recommendation. In *Proceedings of the 31st ACM international conference on advances in geographic information systems*. 1–10.
- [48] Hao Xue, Flora Salim, Yongli Ren, and Nuria Oliver. 2021. MobTCast: Leveraging auxiliary trajectory forecasting for human mobility prediction. *Advances in Neural Information Processing Systems* 34 (2021), 30380–30391.
- [49] Xiaodong Yan, Tengwei Song, Yifeng Jiao, Jianshan He, Jiaotuan Wang, Ruopeng Li, and Wei Chu. 2023. Spatio-temporal hypergraph learning for next POI recommendation. In *Proceedings of the 46th international ACM SIGIR conference on research and development in information retrieval*. 403–412.
- [50] Dingqi Yang, Daqing Zhang, Vincent W Zheng, and Zhiyong Yu. 2014. Modeling user activity preference by leveraging user spatial temporal characteristics in LBSNs. *IEEE Transactions on Systems, Man, and Cybernetics: Systems* 45, 1 (2014), 129–142.
- [51] Menglin Yang, Zhihao Li, Min Zhou, Jiahong Liu, and Irwin King. 2022. Hicf: Hyperbolic informative collaborative filtering. In *Proceedings of the 28th ACM SIGKDD Conference on Knowledge Discovery and Data Mining*. 2212–2221.
- [52] Menglin Yang, Harshit Verma, Delvin Ce Zhang, Jiahong Liu, Irwin King, and Rex Ying. 2024. Hypformer: Exploring efficient transformer fully in hyperbolic space. In *Proceedings of the 30th ACM SIGKDD Conference on Knowledge Discovery and Data Mining*. ACM, 3770–3781.
- [53] Menglin Yang, Min Zhou, Zhihao Li, Jiahong Liu, Lujia Pan, Hui Xiong, and Irwin King. 2022. Hyperbolic graph neural networks: A review of methods and applications. *arXiv preprint arXiv:2202.13852* (2022).
- [54] Song Yang, Jiamou Liu, and Kaiqi Zhao. 2022. GETNext: Trajectory flow map enhanced transformer for next POI recommendation. In *Proceedings of the 45th International ACM SIGIR Conference on research and development in information retrieval*. 1144–1153.
- [55] Yonghui Yang, Le Wu, Kun Zhang, Richang Hong, Hailin Zhou, Zhiqiang Zhang, Jun Zhou, and Meng Wang. 2023. Hyperbolic graph learning for social recommendation. *IEEE Transactions on Knowledge and Data Engineering* 36, 12 (2023), 8488–8501.
- [56] Fuqiang Yu, Lizhen Cui, Wei Guo, Xudong Lu, Qingzhong Li, and Hua Lu. 2020. A category-aware deep model for successive POI recommendation on sparse check-in data. In *Proceedings of the web conference 2020*. 1264–1274.
- [57] Quan Yuan, Gao Cong, Zongyang Ma, Aixin Sun, and Nadia Magnenat Thalmann. 2013. Time-aware point-of-interest recommendation. In *Proceedings of the 36th international ACM SIGIR conference on Research and development in information retrieval*. 363–372.
- [58] Hongyu Zang, Dongcheng Han, Xin Li, Zhifeng Wan, and Mingzhong Wang. 2021. Cha: Categorical hierarchy-based attention for next poi recommendation. *ACM Transactions on Information Systems (TOIS)* 40, 1 (2021), 1–22.
- [59] Lu Zhang, Zhu Sun, Ziqing Wu, Jie Zhang, Yew Soon Ong, and Xinghua Qu. 2022. Next Point-of-Interest Recommendation with Inferring Multi-step Future Preferences. In *IJCAI*. 3751–3757.
- [60] Lu Zhang, Zhu Sun, Jie Zhang, Horst Kloeden, and Felix Klanner. 2020. Modeling hierarchical category transition for next POI recommendation with uncertain check-ins. *Information Sciences* 515 (2020), 169–190.
- [61] Qianru Zhang, Honggang Wen, Wei Yuan, Crystal Chen, Menglin Yang, Siu-Ming Yiu, and Hongzhi Yin. 2025. HMamba: Hyperbolic Mamba for Sequential Recommendation. *arXiv preprint arXiv:2505.09205* (2025).
- [62] Zhenyue Zhang and Hongyuan Zha. 2004. Principal manifolds and nonlinear dimensionality reduction via tangent space alignment. *SIAM journal on scientific computing* 26, 1 (2004), 313–338.

Received 20 February 2007; revised 12 March 2009; accepted 5 June 2009